Original Article

Journal of Tissue Engineering
Volume 12: 1–12

DOI: 10.1177/20417314211022242
journals.sagepub.com/home/tej
SAGE

Artificial decellularized extracellular matrix improves the regenerative capacity of adipose tissue derived stem cells on 3D printed polycaprolactone scaffolds

Jana C Blum[1*], Thilo L Schenck[2*], Alexandra Birt[1], Riccardo E Giunta[1] and Paul S Wiggenhauser[1]

Abstract

Ideal tissue engineering frameworks should be both an optimal biological microenvironment and a shape and stability providing framework. In this study we tried to combine the advantages of cell-derived artificial extracellular matrix (ECM) with those of 3D printed polycaprolactone (PCL) scaffolds. In Part A, both chondrogenic and osteogenic ECMs were produced by human adipose derived stem cells (hASCs) on 3D-printed PCL scaffolds and then decellularized to create cell free functionalized PCL scaffolds, named acPCL and aoPCL respectively. The decellularization resulted in a significant reduction of the DNA content as well as the removal of nuclei while the ECM was largely preserved. In Part B the bioactivation and the effect of the ac/aoPCL scaffolds on the proliferation, differentiation, and gene expression of hASCs was investigated. The ac/aoPCL scaffolds were found to be non-toxic and allow good adhesion, but do not affect proliferation. In the in vitro investigation of cartilage regeneration, biochemical analysis showed that acPCL scaffolds have an additional effect on chondrogenic differentiation as gene expression analysis showed markers of cartilage hypertrophy. The aoPCL showed a large influence on the differentiation of hASCs. In control medium they were able to stimulate hASCs to produce calcium alone and all genes relevant investigated for osteogenesis were significantly higher expressed on aoPCL than on unmodified PCL. Therefore, we believe that ac/aoPCL scaffolds have a high potential to improve regenerative capacity of unmodified PCL scaffolds and should be further investigated.

Keywords

Tissue engineering, adipose derived stem cells, regenerative medicine, polycaprolactone scaffolds, osteogenesis, chondrogenesis

Date received: 26 January 2021; accepted: 17 May 2021

Introduction

Various autologous patient-specific transplants are used in craniofacial surgery to reconstruct bone or cartilage defects resulting from trauma, surgical tumor resection, or repair of congenital malformation.[1] The advantage of autologous grafts is based on their biological activity and lack of immunological adverse reaction. But cartilage transplants as well as bone grafts are accompanied by negative aspects such as a donor site morbidity, shortage of donor tissue, difficult anatomical adoption to recipient site, and risk of later deformity.[2,3] So far, no ideal solution for the therapy of these defects has been found.[4,5] However artificial tissue grafts created by means of tissue engineering and regenerative medicine can be a promising alternative.[6] The basic principle of manufacturing artificial, biologically activated replacement material

[1]Department of Hand Surgery, Plastic Surgery and Aesthetic Surgery, Ludwig Maximilian University of Munich, Munich, Germany
[2]Department of Breast Surgery, Plastic Surgery and Aesthetic Surgery, Frauenklinik Dr. Geisenhofer GmbH, München, Germany

*These authors contributed equally to this work.

Corresponding author:
Paul S Wiggenhauser, Department of Hand Surgery, Plastic Surgery and Aesthetic Surgery, Ludwig Maximilian University of Munich, Pettenkoferstrasse 8a, Munich, Bavaria 80336, Germany.
Email: severin.wiggenhauser@med.uni-muenchen.de

is the combination of cells, growth factors, and biomaterials.[7] In order to achieve a physiological replacement, there are many requirements regarding features of applied biomaterials such as sufficient mechanical stability, shape maintenance, and degradability by the body.[8] It is also important to imitate the biological macro and microenvironment to enable good cell adhesion, proliferation, migration, or invasion into the biomaterials. Currently, tissue-engineering approaches consist mainly of two material groups: natural and synthetic scaffolds.[9] So far, tissue derived extracellular matrix (ECM) scaffolds, produced by decellularization of mostly animal cartilage or bone, have been used in the category of naturally produced biomaterials. But the clinical application of xenogenic grafts in humans yields a challenge due to its immunogenicity.[10,11] On the other hand, representing a natural microenvironment is an advantage of promoting chondrogenesis and osteogenesis of various cells, including human adipose derived stem cells (hASCs).[9,12,13] However, the synthetically manufactured scaffolds, made from polycaprolactone (PCL) or poly-L-lactic acid (PLA), receive more and more attention in tissue engineering research as those promise to overcome limitations regarding unsatisfactory mechanical properties and long-term stability of ECM scaffolds.[8] Polycaprolactone (PCL) has higher benefits, due to its FDA approval, biodegradability, biocompatibility, and long-term stability.[3,7,14] Furthermore, the material is compatible with 3D printing and enables production of individually shaped 3D scaffolds made from this biomaterial. This is a big advantage especially in the reconstruction in craniofacial surgery, since complex geometric frameworks are required. As pure PCL is not sufficient to achieve a satisfactory differentiation of hASCs into cartilage or bone tissue,[1,3,9] there were many trials to combine the advantage of natural and synthetic scaffolds to imitate a natural environment by maintaining stability. A number of approaches have been developed to overcome the lack of biocompatibility, as PCL has already been coated or incorporated with various differentiation inductive substances like growth factors, antibodies, or ECM proteins, for example, chondroitin sulfate for chondrogenic differentiation or calcium phosphate for osteogenic differentiation.[13,15–18] Despite of positive results of previous studies, completely bioactivated tissue engineered scaffolds have not been achieved and there is still need for improvement. Compared to coating with ECM particles or proteins, cell-derived ECM produced directly on scaffolds is believed to be advantageous due its more complete microstructure.[19,20]

ASCs are proved beneficial due to their relatively easy collection from donor's liposuctions, multilineage differentiation, and their occurrence in higher concentration when compared to mesenchymal stem cells in bone marrow.[21,22]

The aim of this study was to build artificial cell-derived cartilage and bone ECM by the use of hASCs and PCL scaffolds. We believe that cell-derived ECM on PCL produced by decellularization of previously differentiated constructs should create functionalized scaffolds and offer the advantage of both natural as well as synthetic scaffolds. In this study we hypothesized that activated chondrogenic and osteogenic PCL scaffolds (ac/aoPCL) could provide an appropriate microenvironment that promotes adhesion, viability, proliferation, and differentiation of hASC for cartilage and bone engineering and that is superior to unmodified PCL (uPCL) scaffolds.

Materials and methods

Manufacture of scaffolds

PCL scaffold. PCL scaffolds were produced by Bellaseno GmbH (Leipzig, Germany) in very high-resolution lattice-based structures using melt-extrusion technology combined with medical-grade FDA-approved material. Using its custom-built Yasham additive manufacturing platform, Bellaseno can reproducibly and routinely manufacture scaffolds with unit cell sizes down to about 1 mm that are suitable for high-end tissue engineering approaches. Hence, we obtained disk-shaped scaffolds that had a height of 1 mm and a diameter of 5 mm. The pore geometry was square based with a pore size of 300 µm. All scaffolds were sterilized with 70% ethanol for 1 h and subsequently with UV-light from both sides.

Isolation of ASC. Human adipose tissue derived stem cells (hASCs) were sourced from patients undergoing liposuction procedures or tummy tuck at the Department of Hand, Plastic and Aesthetic Surgery of the Ludwig-Maximilians-University. Written informed consent was obtained by all patients prior to the operations. The study was approved by the institutional ethics committee with registration number 17-046. The isolation protocol from Bunnell et al.[23] was modified, by not using a lysis buffer. The cells were expanded in standard culture medium (Dulbecco's modified Eagle's medium (DMEM): #11971-025, Biochrom, Germany) supplemented with 10% fetal bovine serum (FBS: INV10270-106 Gibco, Thermo Fisher Scientific, USA), 1% Pen/Strep (A2213, Biochrom, Germany), and 1% Amphotericin B (A2612, Biochrom, Germany). To ensure that the cells isolated from the lipoaspirate were ASCs, their multilineage potential was confirmed by differentiating into adipogenic, osteogenic, and chondrogenic cells with StemMACS™ differentiation medium (Miltenyi Biotec, Germany).

Seeding and production of hASC derived ECM on scaffold (part A). The PCL scaffolds were placed in 24-well plates. Before seeding, all hASCs were expanded in standard culture medium in a monolayer until reaching 80%–90%

confluence. The ASCs were seeded at passage 1 with a density of 2.5×10^5 cells/scaffold. Twenty-five microliter of the cell suspension was added dropwise on top of the scaffold without contacting the scaffold. The cell seeded scaffolds were incubated for 4 h at 37°C, 5% CO_2 to allow adhesion. Then 1 ml of standard culture medium was added. After 7 days of cultivation and proliferation, the scaffolds were transferred to a new well to remove non-adherent cells. To improve the differentiation, they were cultured in StemMACs ChondroDiff Media (#130-091-679, Miltenyi Biotec, Germany) respectively. StemMACS™ OsteoDiff Media (#130-091-678, Miltenyi Biotec, Germany) supplemented with 1% P/S and 1% Amphotericin B for 6 weeks. The medium was changed as needed every 2–3 days a week. At the end of this period, the cell loaded native scaffolds underwent decellularization process to remove all vital cells and create the ac/aoPCL scaffolds.

Production of activated chondrogenic/osteogenic PCL (part A). The cell loaded (native) scaffolds were decellularized using a chemical lysis of cells and enzymatic digestion of DNA. We decided to use sodium deoxycholate because it showed a higher biocompatibility compared to sodium dodecyl sulfate.[24] In this process, 2% sodium deoxycholate (SD: D6750, Sigma-Aldrich, USA) was used to solubilize the cell membrane. Cell loaded scaffolds were incubated in SD for 1 h by shaking at room temperature. Afterwards the samples were washed in phosphate buffered saline (PBS: L1825, Biochrom, Germany). To remove and avoid an agglutination of DNA, the scaffolds were incubated in 2 kU/ml DNase (D4263-1VL, Deoxyribonuclease I from bovine pancreas: Sigma-Aldrich, USA) at 37°C for 2 h, followed by a washing step with PBS. To reach a better degradation of cells and genetic material, this procedure was repeated two times. This procedure was developed by combining the protocols from Sun et al.[10] and Partington et al.[25] Subsequently the activated PCL scaffolds (ac/aoPCL) were analyzed by various biochemical assays and imaging techniques. For further use they were stored in PBS with 1% P/S and 1% Amphotericin B at +4°C (Figure 1).

Investigation of the influence of ac/aoPCL on hASC (part B). In Part B, three different types of scaffolds, acPCL, aoPCL, and uPCL, were compared. Unmodified PCL scaffolds referred to untreated scaffolds as they were purchased from manufacturer. The scaffolds were seeded again with ASCs as previously described under 2.1.3. Three days after seeding the induction group ($n = 3$) was incubated in chondrogenic respectivley osteogenic differentiation medium, while the control group ($n = 3$) was cultured in standard culture medium. Both induction medium and culture medium were used to investigate whether the activated scaffolds in culture medium can induce the differentiation of hASCs or whether they can enhance it in induction medium. During cultivation for 14 or 21 days, medium was changed three times per week (Figure 1).

Biochemical analyses

For sample preparation, all cell seeded scaffolds were weighted and transferred to 2 ml safe-lock reaction tubes (Eppendorf, Germany) containing 300 µl of PBS. The 3D constructs were homogenized by using a tissue lyser (Tissue Lyser LT, Thermo Fisher Scientific, USA) for 20 min at 50 Hz with a 7 mm stainless steel bead. The sample was then centrifuged for 30 s at 1000 rpm and 200 µl of supernatant was aliquoted at −20°C for further use. The remaining 100 µl were digested with 500 µl 125 µg/ml proteinase K (P2308, AppliChem, Germany) overnight at 56°C for DNA and glycosaminoglycan assays. Enzymatic activity was stopped by cooling samples to −20°C. Thus one third of the homogenized scaffold solution was used for each biochemical analysis. Subsequently the amount was extrapolated to 100% of probe size and normalized to PCL scaffold weight. Each biochemical analysis was performed in biological triplicates and technical duplicates. All assays were evaluated against the baseline of the respective group. The baseline was defined as the negative control. Accordingly, PCL without cells for the uPCL-group and the activated PCL scaffold without cells for the ac/aoPCL-group.

DNA content. A Pico Green assay was used to measure the double-stranded DNA content and thus draw conclusions about the cell number and proliferation. For this, the samples previously digested in proteinase K (P2308, AppliChem, Germany) were centrifuged at 6000 rpm for 5 min. The samples were diluted 1:3 with Tris-EDTA (TE)-buffer (A8569,0500, AppliChem, Germany) and 100 µl each was placed in a 96-well plate. Finally, 100 µl 0.005% Quant-iT™ PicoGreen™ ds DNA Reagent (P7581, Thermo Fisher Scientific, USA) color solution was added and the DNA content was determined using a fluorescent plate reader (Infinite Pro 200, Tecan, Switzerland) at extinction $\lambda = 504$ nm and emission $\lambda = 550$ nm. The DNA content was calculated using a dsDNA standard curve, which was generated by self-isolated DNA using a spectrophotometer (NanoPhotometer, Implen, Germany). Finally the measured amount of DNA was extrapolated to 100% of probe size and normalized to PCL scaffold weight.

Glycosaminoglycan content. Dimethylmethylene blue (DMMB) assay, staining of chondroitin sulfate, was applied to quantify glycosaminoglycans (GAGs) within the samples. The digested probes were centrifuged at 10.000 rpm for 5 min. Fifty microliter of supernatants was transferred to a new 2 ml reaction tube and treated with 500 µl DMMB working solution (#341088, Sigma Aldrich,

USA), which was produced according to Barbosa et al.[26] All tubes were put on a linear shaker for 45 min at 600 rpm to allow complexation of GAGs with DMMB. The samples were then centrifuged at 5000 rpm for 10 min so the complexes settled to the bottom. In the next step, the entire liquids were carefully removed with a pipette and the decomplexation solution[26] was added to dissolve the complexes. After extensive shaking the absorbance was measured in duplicates at wavelength of $\lambda = 656$ nm on a 96 well plate using a plate reader (Infinite 200 Pro, Tecan, Germany). Calibration was done by using a standardized calibration curve made from chondroitin sulfate (#5197.1, Sigma-Aldrich, USA) that was treated analogously to homogenized samples. Finally the measured amount of GAGs was extrapolated to 100% of probe size and normalized to PCL scaffold weight.

Hydroxyproline content. The newly produced total hydroxyproline content and thus collagen was quantified using a colorimetric hydroxyproline determination kit (MAK008, Sigma-Aldrich, USA). For this, 100 µl of the sample supernatant was hydrolyzed with 100 µl of 25% hydrochloric acid (X897.1, Carl Roth, Germany) for 24 h at 99°C. Furthermore, the hydrochloric acid was stopped with activated charcoal (C4386, Sigma-Aldrich, Germany) and the samples were evaporated at 60°C. Based on the manufacturer's instructions, the assay was further performed by adding ChloramineT/Oxidation Buffer Mixture and diluted DMAB reagent to the samples. Finally, the absorbance was measured at 560 nm and the samples were extrapolated against hydroxyproline standards. Finally the measured amount of hydroxyproline was extrapolated to 100% of probe size and normalized to PCL scaffold weight.

Calcium content. The calorimetric QuantiChrom™ Calcium assay kit (DICA-500, Bioassay Systems, USA) was used to quantify the amount of newly produced calcium. Therefore, calcium was extracted with 0.5 N HCL at 4°C for 24 h and then centrifuged for 1 min at 13.500 rpm. Subsequently, the assay was performed according to manufacturer's instructions by adding 200 µl working reagent to each sample (5 µl) and by measuring the absorbance at 612 nm. The total calcium content was calculated using a standard curve as described in the instructions. Finally the measured amount of calcium was extrapolated to 100% of probe size and normalized to PCL scaffold weight.

Live/dead-assay

To optically evaluate the amount of DNA left on ac/aoPCL-scaffolds, cell viability and distribution a live/dead fluorescence staining was performed. For this, the scaffolds after decellularization resp. recellularization on day 3 were first transferred to 24-well plate containing live staining solution with 8 µg/ml fluorescein diacetate (FDA: F7378, Sigma Aldrich, USA) for 5 min and afterwards into 20 µg/ml propidium iodide (PI: P4864, Sigma Aldrich, USA) dead staining solution for 5 s. Both staining solutions were made in serum-free without phenol red DMEM (Gibco, Thermo Fisher Scientific, USA). After rinsing with PBS digital fluorescent pictures were taken with inverted epifluorescence microscope (Zeiss Axio Observer, Zeiss, Germany). The Z-stack of the images was reconstructed into a 3D image using an image processing program (FIJI Image J, V.1.52I).

Histology

Scaffolds before and after decellularization were stained to show the extracellular matrix and nuclei. For histological examination, scaffolds were directly fixed in 4% formaldehyde (MicroCross, Germany), completely embedded in paraffin blocks and then cut in 5 µm-thick serial sections with Microm HM 340E (Thermo Fisher Scientific, USA). Staining for chondrogenic extracellular matrix was performed by incubating in alcian blue (#3082.2, Carl-Roth, Germany) staining solution for 1 h and the nuclei were stained with nuclear red for 5 min according to standard protocols. To visualize osteogenesis, sections were stained in Alizarin red S (A5533, Sigma-Aldrich, USA) over night. Afterwards nuclei were stained with 4′,6-diamidino-2-phenylindole (DAPI: D1306, Invitrogen, Thermo Fisher Scientific, USA) according to manufacturer's protocol.

Gene expression analysis

To assess gene expression profiles, real time polymerase chain reaction (RT-PCR) was performed. Therefore, scaffolds were snap frozen in RNA Later (#160027967, Qiagen, Germany) and stored at −80°C. The total RNA extraction was carried out according to manufacturer's protocol with RNAeasy Mini Kit (#74104, Qiagen, Germany). In the first step, 350 µl RLT buffer (10 µl β-Mercaptoethanol per 1 ml RLT buffer) and a stainless steel bead was added to the probes in each tube. Subsequently, a TissueLyser at 15 Hz was used for 30 s to homogenize the samples, which were then centrifuged for 3 min at 14,000 rpm. In the next step, the supernatant was purified by using the RNeasy Mini Kit pursuant according to manufacturer's protocol. The measurement of RNA concentration and purity obtained was done using a nano-photometer (Implen, Germany). The subsequent cDNA synthesis was carried out per Transcriptor First Strand Kit (#4379012001, Roche, Switzerland) in a thermocycler (T-Professional Basic thermocycler, Biometra (Analytik Jena), Germany. Thereon, RT-PCR was conducted by using 5 µl of each cDNA sample and the InnuMIX DS Green Standard Kit (#012-18, Analytik Jena, Germany) in a Real-Time-Thermocycler (qTOWER^{3}G, Analytik Jena, Germany). All primers used for this experiment were

Table 1. Primer sequences.

Gene	Name	Sequence	
ACAN	Aggrecan core protein	Left	5-cctcccccttcacgtgtaaaa-3
		Right	5-gctccgcttctgtagtctgc-3
SOX9	Transcription factor SOX-9	Left	5-gtacccgcacttgcacaac-3
		Right	5-tctcgctctcgttcagaagtc-3
COL1A1	Collagen type I alpha 1 chain	Left	5-gggattccctggacctaaag-3
		Right	5-ggaacacctcgctctcca-3
COL2A1	Collagen type II alpha 1 chain	Left	5-gtgaacctggtgtctctggtc-3
		Right	5-tttccaggttttccagcttc-3
Col10a1	Collagen type X alpha 1 chain	Left	5-caccttctgcactgctcatc-3
		Right	5-ggcagcatattctcagatgga-3
ITGA11	Integrin subunit alpha 11	Left	5-cttttcctcgcacgtggt-3
		Right	5-gctccattccagtcataggc-3
COL9A1	Collagen type IX alpha 1 chain	Left	5-gagcttggccgtgtaggac-3
		Right	5-aaagccaattgttcctctgg-3
ALPL	Alkaline phosphatase	Left	5-cctgccttactaactccttagtgc-3
		Right	5-cgttggtgttgagcttctga-3
SPP1	Osteopontin secreted phosphoprotein 1	Left	5-gagggcttggttgtcagc-3
		Right	5-caattctcatggtagtgagttttcc-3
GAPDH	Glyceraldehyde-3-phosphate dehydrogenase	Left	5-gactaaccctgcgctcctg-3
		Right	5-gcccaatacgaccaaatcag-3
HPRT1	Hypoxanthine-guanine phosphoribosyltransferase 1	Left	5-tgaccttgatttattttgcatacc-3
		Right	5-cgagcaagacgttcagtcct-3

listed in Table 1 and designed with Sigma-Aldrich's OligoArchitect™ Primer software. First, the denaturing was done at 95°C for 2 min, followed by amplification in 50 cycles of 95°C for 30 s, 60°C for 1 min, 68°C for 30 s. The relative gene expression was normalized to the corresponding HouseKeepingIndex, consisting of the average of GAPDH and HRPT1. Afterwards, the transcript levels were calculated as $w = 2^{-\Delta\Delta Ct}$, in which $\Delta\Delta Ct = \Delta Induction - \Delta Control$ was calculated from the ac/ao-PCL- and uPCL-group.

Statistical analysis

All data from control and experimental groups were analyzed using the unpaired *t*-test in Excel (Microsoft Office 2016, USA) respectively. Two-way ANOVA in SPSS software (IBM SPSS Statistics 25, USA), with statistical difference set as $p < 0.05$. All values were presented as mean ± standard deviation.

Results

Part A: Production of an extracellular matrix 3D-printed PCL scaffold

Effectivity of decellularization procedure. In this respect, histology showed that almost no cell nuclei were left in both differentiation groups and thus almost all cells were removed (Figure 2). A PicoGreen was carried out for a more precise assessment of the remaining amount of DNA on the decellularized scaffolds aoPCL and acPCL respectively. In both differentiation groups, this showed a significant reduction in the genetic material with only a minimal amount of DNA remaining (Figure 3(a) and (d)).

Influence of decellularization on composition/structure of ECM. Both histology and biochemical assays were performed to determine the influence of decellularization on the composition of the cell-derived ECM. Regarding the chondrogenic differentiation, alcian blue optically showed no difference in the intensity of the coloring and also in the amount of GAG (Figure 2). The DMMB assay, which is used to detect GAGs, underpins the qualitative findings of histology. There was no significant loss of GAGs due to decellularization (Figure 3(b)). DMAB, on the other hand, showed a significant difference before and after decellularization and thus also indirectly a loss of collagen (Figure 3(c)).

Regarding the osseous scaffolds, the histology showed only a slight difference in the color strength of alizarin Red coloring (Figure 2). It can therefore be assumed that the basic osteogenic structure of the native scaffolds has been preserved. The calcium assay reflects the results of the histology. An insignificant decrease in the amount of calcium remaining was visible (Figure 3(e)).

Part B: Evaluation of the effect on the ASCs

Recellularization. After 3 days in culture, the scaffolds newly populated with hASC were stained with Live/Dead. In the pictures in Figure 4(b) to (d) almost all cells are

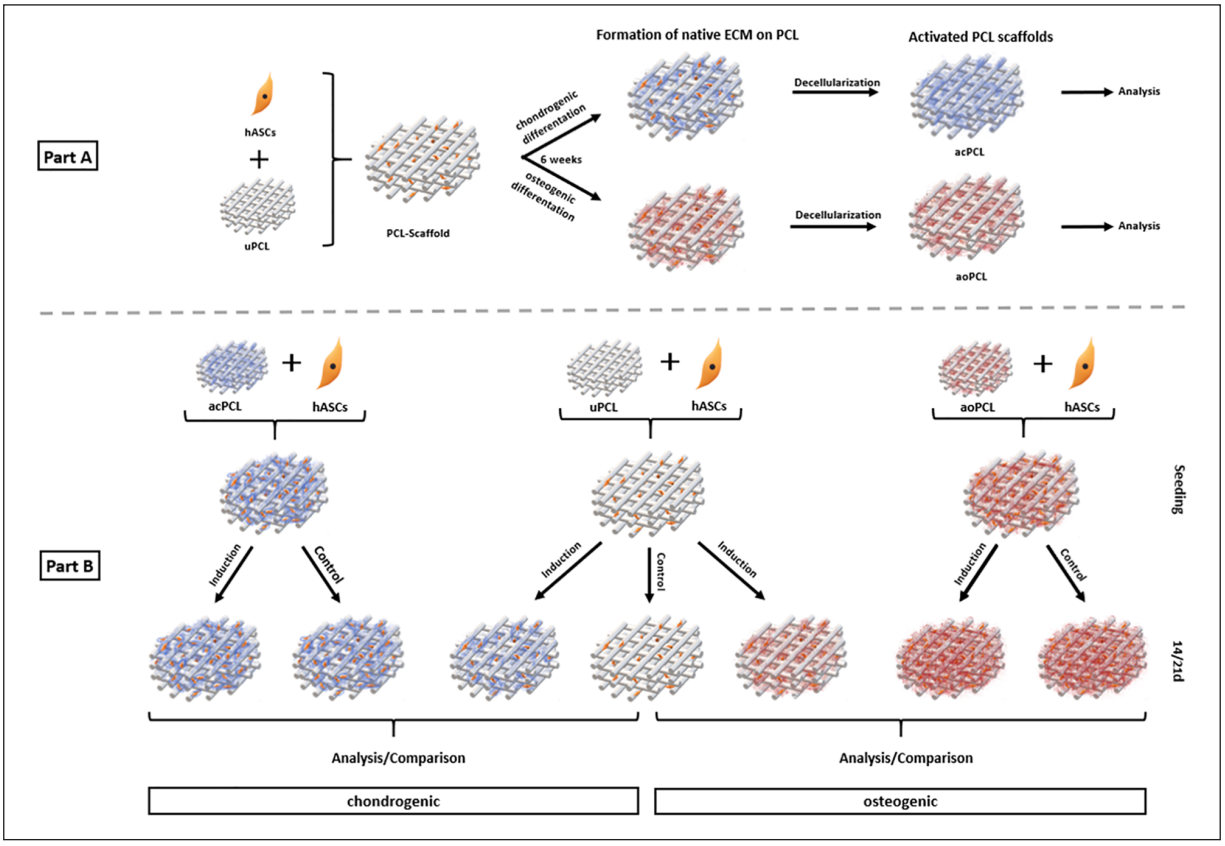

Figure 1. Schematic drawing of the experimental approach: Part A manufacturing of activated PCL scaffolds and Part B evaluation of ac/aoPCL an uPCL scaffolds in in vitro setup.

stained alive and hardly any dead cells can be seen. Additionally, ac/aoPCL scaffolds showed a clearly higher cell number compared to uPCL scaffolds and cells were homogeneously distributed on ac/aoPCL scaffolds, whereas cells did not fill pores in the uPCL scaffolds.

Biochemical analysis. A significant promotion of the proliferation by both the chondrogenic and the osteogenic differentiation medium could be found in the Pico Green assay, shown in ANOVA analysis when comparing induction with control group. In addition, there is a significant higher dsDNA content in the osteogenic induction compared to control on day 21 of both scaffold groups, shown by *t*-test analysis. An insignificant increase of dsDNA was shown in the osteogenic induction group. In chondrogenesis, however, there was a significant difference between induction and control on day 14 in the uPCL group and on day 21 in the acPCL group (Figure 4(e) and (f)).

In the hydroxyproline-assay there was no significant difference between acPCL-scaffold and uPCL-scaffold in the control medium. In the induction group however, there was a significant increase in the amount of newly produced hydroxyproline in the acPCL-group compared to the uPCL-group at both time points. In the acPCL-group, a significantly higher content of hydroxyproline in the differentiation medium compared to the normal culture medium was revealed on both days 14 and 21. This significant effect can only be seen on day 14 in the PCL group. Statistical ANOVA analysis of the hydroxyproline assay also showed a significant influence of the medium and the scaffolds variant (Figure 5(a)). This also showed a significant influence of the medium and the day on GAG content. In addition, *t*-test shows only a significant higher number of GAGS in the acPCL group when comparing induction and control on day 21. The other groups show only a slight difference between the two media (Figure 5(b)).

The calcium assay was performed to quantify osteogenesis. The *t*-test showed a significantly higher calcium content on the aoPCL scaffolds than on the uPCL in control medium at both time points. This effect was also shown in the differentiation medium on day 21. When comparing the calcium content on the aoPCL between induction and control group, only a marginal difference can be seen (Figure 5(c)).

Gene expression analysis. Regarding chondrogenic differentiation, there is a significant difference in ITGA11 and COL9A1. The ACAN, COL2A1, COL10A1 genes are highly regulated in both groups. ACAN and COL10A1 are

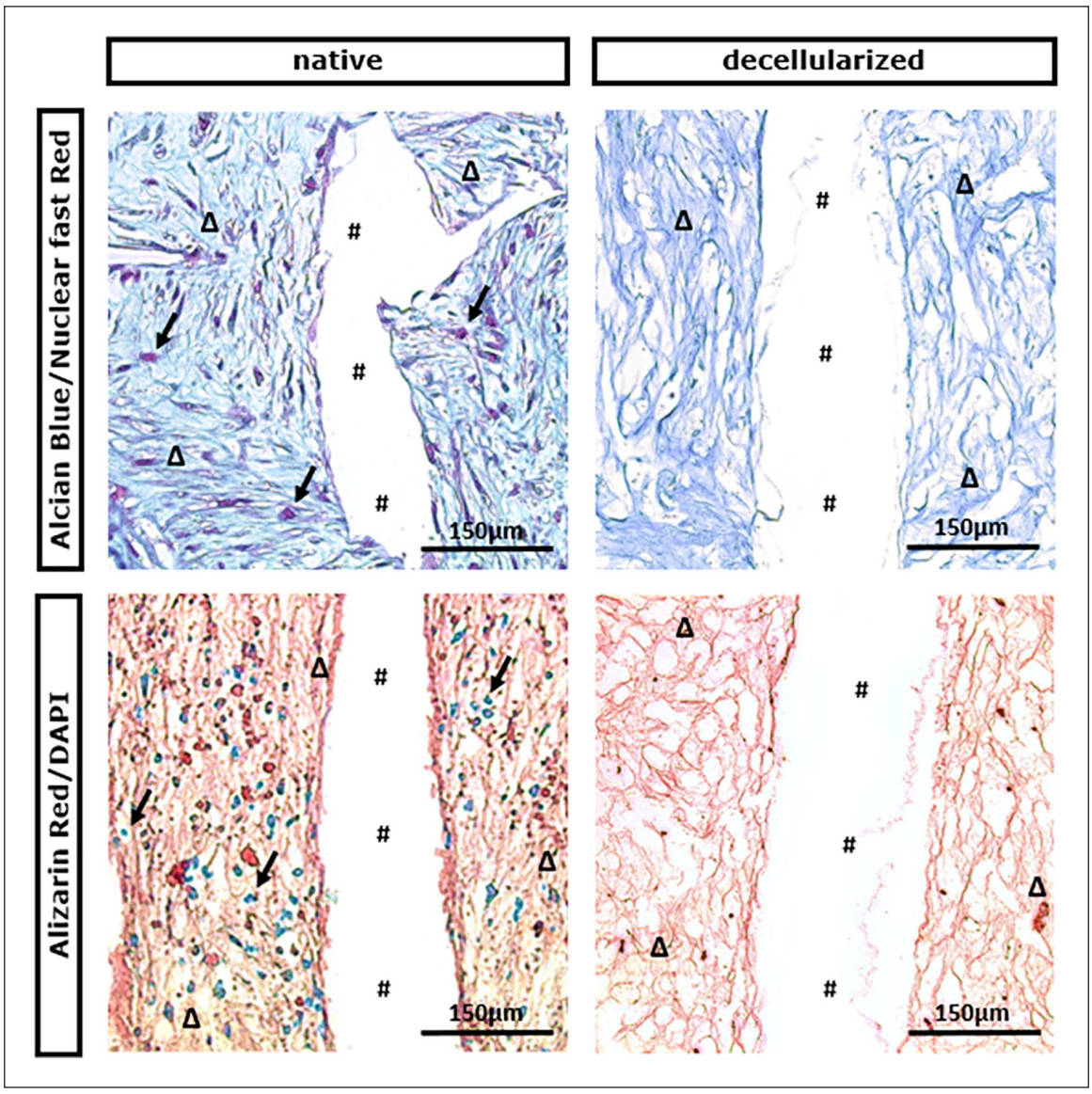

Figure 2. Assessment of decellularization process of acPCL (upper row) and aoPCL (bottom row) by specific histology. Images show removal of cells (↓) and persistence of tissue specific ECM (Δ; blue = GAGs, red = calcium deposits). The melted PCL filaments are marked with **#**.

insignificantly higher in the uPCL group but not significant. In contrast, COL2 tended to show higher expression in the acPCL group. Concerning the gene SOX9 the expression was almost identical in both groups. In addition, COL1A1 is downregulated in both groups with no significant difference (Figure 6(a)).

The qPCR of osteogenic differentiation made on day 14 shows significantly higher gene expression in the aoPCL group for all genes except COL10A1 compared to the uPCL group. ACAN is down regulated for both, but significantly stronger for the uPCL scaffolds. COL1A1, COL9A1, SPP1, and ALPL are significantly up-regulated in the aoPCL group, whereas these genes are down-regulated in the uPCL group (Figure 6(b)).

Discussion

This study was intended to combine advantages of natural decellularized tissue and 3D printable PCL scaffolds. Decellularized tissues have gained increasing attention due to their excellent biocompatibility and PCL has been studied due to its 3D printability, stability, and controllable biodegradability.[4,27] We generated functionalized PCL by decellularization of chondrogenic and osteogenic differentiated PCL constructs, termed aoPCL and acPCL, in part A of this study. In part B, we hypothesized that activated PCL (aoPCL and acPCL) provides a biological microenvironment superior to unmodified PCL in terms of biological compatibility, proliferation, and differentiation.

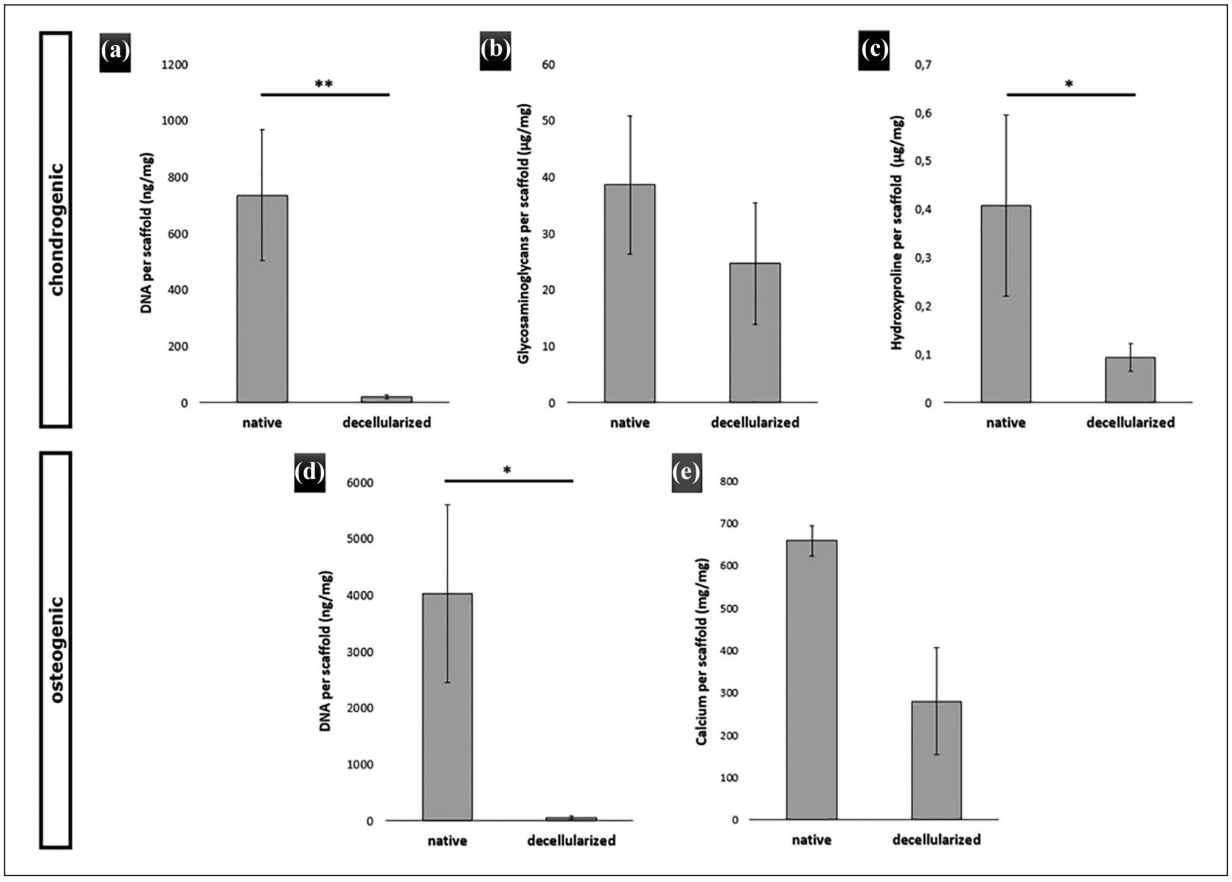

Figure 3. Biochemical analysis for chondrogenic (a, b, c) and osteogenic (d, e) differentiated ECM before (native) and after decellularization process: cartilage ECM was measured with Hydroxyproline assay (Collagen) and DMMB assay (GAGs), whereas osseous ECM by calcium assay. Cell number was quantified using Pico Green assay (amount of DNA per scaffold).
Data are shown as mean value ± SD, $n = 3$.
*$p < 0.05$. **$p < 0.01$.

The literature research for part A of this study found several studies that described decellularization protocols with SD and DNAse to preserve ECM while effectively removing cells.[28] Therefore we adopted those protocols to our experimental approach. Finally, both histology and the pico-green assay showed that chemical and enzymatic decellularization was largely successful in removing nuclei and DNA in both ways of differentiation. In many studies it remains controversial how much persistent genetic material is still acceptable after decellularization. Some groups defined a lack of nuclear material in histological staining as acceptable and others defined a threshold below 50 ng/mg DNA by ECM dry weight.[29,30] Regarding the amount of remaining ECM proteins, there was no significant decrease of calcium on the osseous activated PCL scaffolds neither in the biochemical assay nor in the Alizarin red staining. The decellularization of cartilaginous ECM can also be considered successful. Histology showed a roughly equal content of GAGs before and after decellularization, which is underlined by the DMMB. Unfortunately, a significant loss of hydroxyproline was measurable. Nevertheless, the decellularization protocol seems to have achieved a good balance in the removal of DNA and the retention of ECM matrix.

Subsequently in Part B of this study we compared the biological compatibility, proliferation, and differentiation of hASCs on activated cartilaginous and osseous PCL with unmodified PCL. Regarding the biological compatibility, the adhesion, vitality, and differentiation of hASCs was investigated. The live/dead staining of hASCs on day 3 suggests that the ac/aoPCL scaffolds are nontoxic to hASCs and provide a good microenvironment for adhesion and are favorable compared to uPCL, also shown by the high gene regulation of Integrin 11 in uPCL scaffolds. Regarding proliferation, after 14 and 21 days there was no significant difference in the amount on DNA compared ac/aoPCL to uPCL scaffolds. However, there was a significant influence of the induction media on DNA quantity.

Furthermore, ECM owns the ability to modulate cell differentiation by influencing mechanical and chemical signaling pathways.[17,31] However, the use of isolated ECM components such as collagen or calcium could

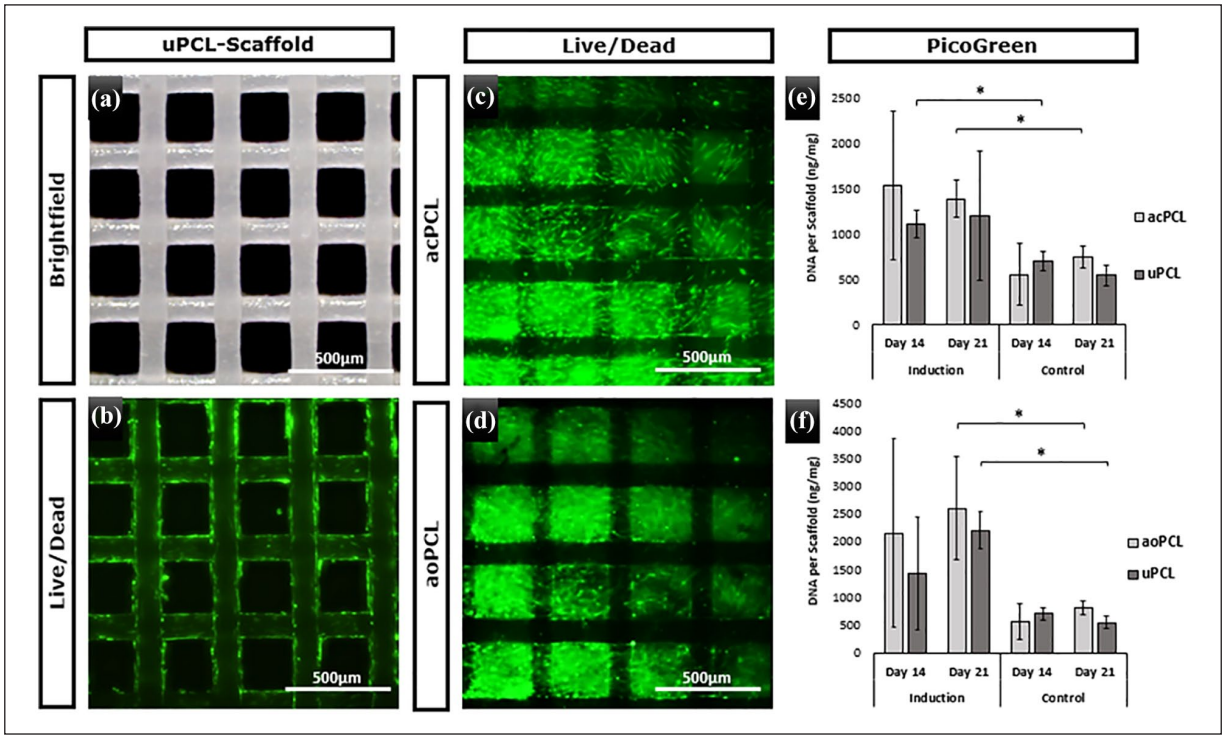

Figure 4. Scaffold geometry of unmodified PCL scaffolds is illustrated with a bright-field image (a). Cell adherence and viability are demonstrated for uPCL (b), acPCL (c), and aoPCL (d) scaffolds by live/dead staining at day 3. Finally, after 14 and 21 days proliferation was quantified by Pico Green assay (amount of DNA per scaffold) for differentiation and control medium for acPCL (e) and aoPCL(f).
Data are shown as mean value ± SD, $n = 3$.
*$p < 0.05$.

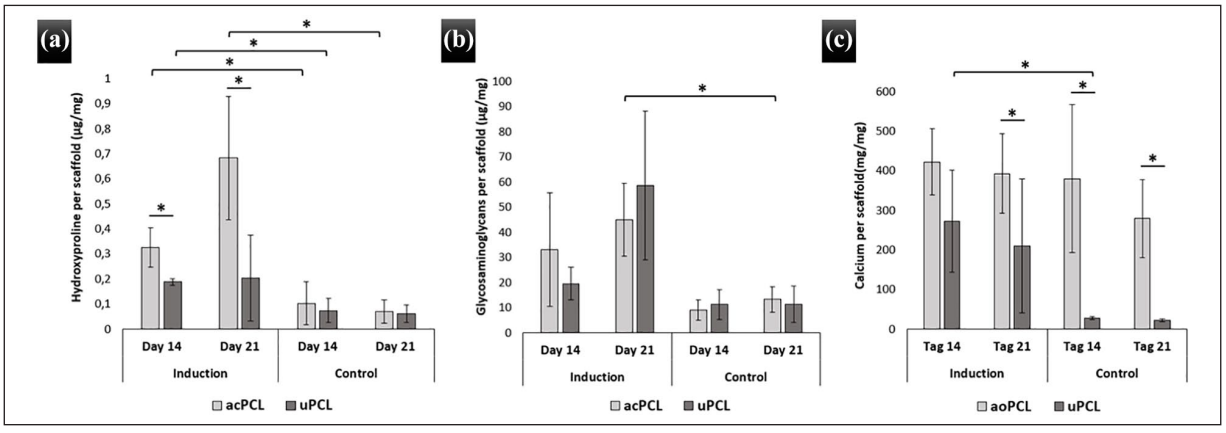

Figure 5. Biochemical Analysis of ECM produced by hASC on activated PCL scaffolds and uPCL scaffolds in both differentiation and standard culture medium: (a) demonstrates the results of the Hydroxyproline, (b) of the DMMB, and (c) of the calcium assay. Untreated PCL scaffolds served as controls.
Data are shown as mean value ± SD, $n = 3$.
*$p < 0.05$.

not reproduce the complex structure and mixture of the proteins in experiments and thus the desired effects as differentiation could not be achieved.[32,33] ECM provides a unique 3D structure, built from tissue-specific components, and thus provides optimal conditions for cell adhesion and proliferation and its repopulation with appropriate cells may lead to formation of the required tissue.[21,29] Therefore, this study investigated the influence of activated PCL compared to uPCL on differentiation capacity of hASCs by various biochemical assays and PCR. Among others, different subtypes of collagens synthesized at different time points in both lineages of differentiations were

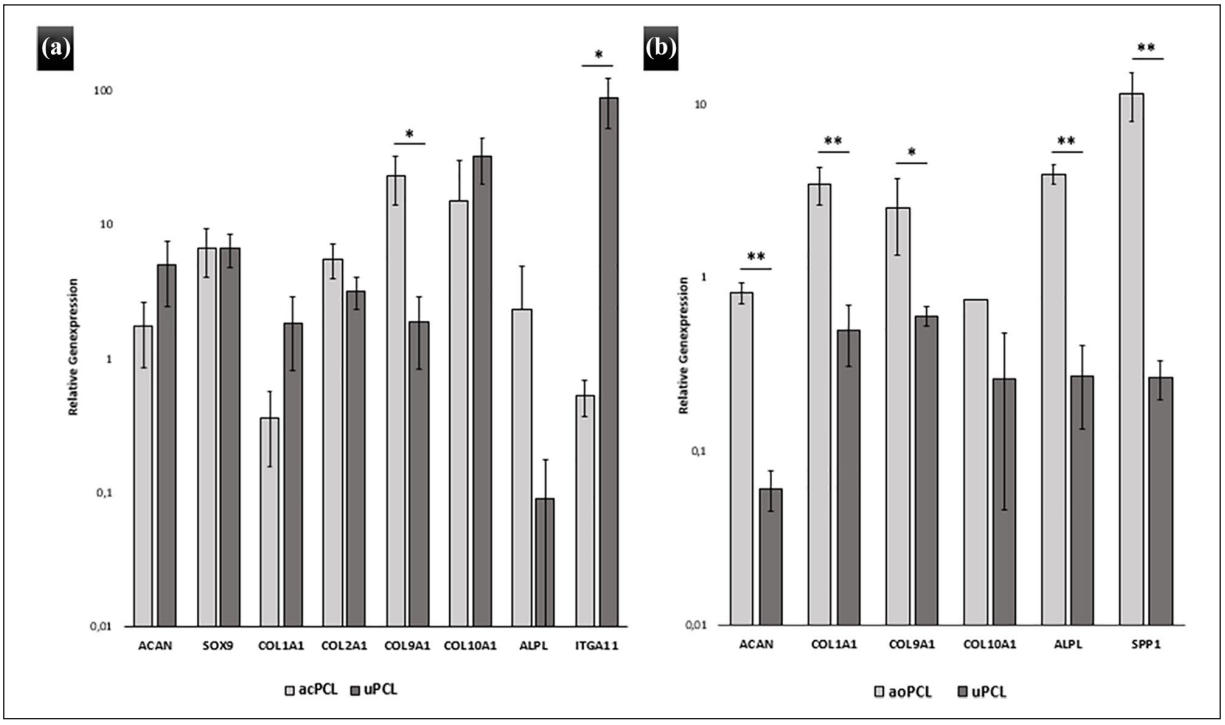

Figure 6. Graphs showing relative gene expression profiles of hASCs cultivated on acPCL (a) and aoPCL (b) scaffolds with uPCL scaffolds as controls using ΔΔCT-approach calculated with difference of specific gene expression to housekeeping gene index and difference of cartilaginous and osteogenic induced scaffolds to non-induced scaffolds. Hence all data show gene expression changes of specific differentiation process.
Data are shown as mean value ± SD, $n = 3$.
*$p < 0.05$. **$p < 0.01$.

examined. Additionally, further markers of differentiation, for example, ALPL that has different effects in chondrogenesis and osteogenesis, were examined.[34,35]

One part of this study investigated the influence of acPCL compared with uPCL in vitro. The biochemical assays showed an insignificant increase in cartilage-specific proteins, including GAGs and hydroxyproline, in the induction group on both scaffold groups compared to the control group. The biochemical assays also showed that acPCL alone is not sufficient to induce chondrogenic differentiation. Nevertheless, an additive effect of acPCL in the induction group on ECM production is visible. A real-time PCR on day 14 was performed to investigate the changes in cartilaginous ECM production by the hASCs in more detail. As a marker of early chondrogenesis, the transcription factor SOX9 causes an upregulation of cartilage-specific structural proteins including COL1A1 and COL2A1 which are markers for condensation and consequently for the initial stage of chondrogenesis.[34] Subsequently, differentiation into chondrocytes leads to the expression of ACAN and COL9A1.[7,36] The results of qPCR show the chondrogenic differentiation ability of hASC on both scaffold groups due to the equal upregulation of the genes expressed during differentiation and maturation into chondrocytes. The expression of COL10A1 and ALPL is considered a sign of hypertrophy and thus the terminal stage of differentiation.[27,37] Regarding these genes, there is one significant difference: COL9A1 was clearly more upregulated on acPCL scaffolds, which is important for the cross-linking of COL2 fibrils and the integration of other cartilaginous structural components.[8,32] In addition, in the uPCL group a downregulation of the ALPL gene was observed, which in contrast was expressed in the acPCL group above 1. This may indicate a differentiation into hypertrophic chondrocytes in the acPCL group. Overall, these results show that activated cartilaginous PCL scaffolds were able to support the chondrogenic differentiation of hASCs.

The other part of this study dealt with the influence of aoPCL on osteogenesis of hASC. The effect of aoPCL scaffolds was surprisingly strong, as they were able to induce calcium secretion by hASCs in normal culture medium, in contrast to unmodified PCL. As in chondrogenesis, it also seems to have an additional effect in osteogenic differentiation media. Since calcium is only one component in bone, RT-PCR was performed to study the gene expression of other important osteogenic components. In the early phase of osteogenesis, expression of COL1 and ALPL occurs.[38] The latter is considered a marker for matrix maturation and decreases in the later

phase of osteogenesis. Subsequently, mineralization takes place, which is characterized by the upregulation of osteopontin (SPP1).[39] The qPCR results underscore the results of the calcium assay, COL1A1, ALPL, and SPP1, which are essential for osteogenic differentiation of hASCs, were significantly higher regulated on aoPCL scaffolds than on uPCL. An upregulation of COL9A1 was also visible in the aoPCL group. One study showed that in COL9A1 knockout mice, skeletal deformities occur and thus COL9A1 has both a regulating and an organizing effect at the growth plate.[40] Furthermore, no differentiation into other tissues was detectable.

The study shows that the chondrogenic and osteogenic activated PCL scaffolds provide a good microenvironment for the hASCs to adhere and proliferate. As hypothesized, ac/aoPCL increase the production of ECM proteins in induction medium and aoPCL could induce osteogenic differentiation of hASCs in culture medium on top of that. Although the current study shows the positive influence of activated PCL scaffolds on the differentiation capacity of stem cells, one limitation is that only an in vitro characterization was performed. In vivo studies must be performed to investigate the clinical applicability of the scaffolds and their influence on tissue regeneration potency on hASCs. Many aspects are of particular importance in this respect. Immunogenicity, angiogenesis, and thus the integration of the scaffolds as well as the mechanical long-term stability, which is particularly important in head and neck reconstruction, play a role in the development of the scaffolds.

Conclusion

In this study we successfully produced a decellularized ECM on innovatively 3D-printed PCL scaffolds that was synthesized by hASCs. The acPCL showed an additive effect on the chondrogenesis of hASCs resulting in more ECM produced by hASCs on the acPCL scaffolds than on uPCL scaffolds. The induction of chondrogenesis by acPCL scaffolds alone could not be achieved. On the other hand, the aoPCL scaffolds induced osteogenic differentiation of the hASCs in culture medium so that differentiation seemed to be possible without further inductive factors. Therefore, chondrogenic an osteogenic activated PCL scaffolds might become an interesting novel technique to bioactivate artificial, 3D printed scaffolds with similar advantages as known from natural decellularized tissue but without the need for a source of natural tissue. Hence, further in vivo experiments should be performed to investigate if our technology allows the bioactivation of scaffolds in a clinically relevant animal model and if it is suitable for clinical application.

Author contributions

W.P. designed and directed the project; B.J. performed the experiments, analysis, and wrote the manuscript. B.A. performed the qPCR. S.T. and G.R. supervised the study. All authors discussed the results and contributed to the final manuscript.

Declaration of conflicting interests

The author(s) declared the following potential conflicts of interest with respect to the research, authorship, and/or publication of this article: W.P. is cofounder and shareholder of BellaSeno GmbH. The other authors declare no conflict of interest.

Funding

The author(s) disclosed receipt of the following financial support for the research, authorship, and/or publication of this article: The study was partially financed by LMU funding programme for research and education (FöFoLe).

ORCID iD

Paul S Wiggenhauser https://orcid.org/0000-0002-6645-5230

References

1. Zhang W and Yelick PC. Craniofacial tissue engineering. *Cold Spring Harb Perspect Med* 2018; 8: a025775.
2. Rettinger G. Risks and complications in rhinoplasty. *GMS Curr Top Otorhinolaryngol Head Neck Surg* 2007; 6: Doc08.
3. Rindone AN, Nyberg E and Grayson WL. 3D-printing composite polycaprolactone-decellularized bone matrix scaffolds for bone tissue engineering applications. *Methods Mol Biol* 2018; 1577: 209–226.
4. Wiggenhauser PS, Schwarz S, Koerber L, et al. Addition of decellularized extracellular matrix of porcine nasal cartilage improves cartilage regenerative capacities of PCL-based scaffolds in vitro. *J Mater Sci Mater Med* 2019; 30: 121.
5. Datta P, Ozbolat V, Ayan B, et al. Bone tissue bioprinting for craniofacial reconstruction. *Biotechnol Bioeng* 2017; 114: 2424–2431.
6. Mellor LF, Nordberg RC, Huebner P, et al. Investigation of multiphasic 3D-bioplotted scaffolds for site-specific chondrogenic and osteogenic differentiation of human adipose-derived stem cells for osteochondral tissue engineering applications. *J Biomed Mater Res B Appl Biomater* 2020; 108: 2017–2030.
7. Dao TT, Vu NB, Pham LH, et al. In vitro production of cartilage tissue from rabbit bone marrow-derived mesenchymal stem cells and polycaprolactone scaffold. *Adv Exp Med Biol* 2019; 1084: 45–60.
8. Li Y, Liu Y, Xun X, et al. Three-dimensional porous scaffolds with biomimetic microarchitecture and bioactivity for cartilage tissue engineering. *ACS Appl Mater Interfaces* 2019; 11: 36359–36370.
9. Hung BP, Naved BA, Nyberg EL, et al. Three-dimensional printing of bone extracellular matrix for craniofacial regeneration. *ACS Biomater Sci Eng* 2016; 2: 1806–1816.
10. Sun Y, Yan L, Chen S, et al. Functionality of decellularized matrix in cartilage regeneration: a comparison of tissue versus cell sources. *Acta Biomater* 2018; 74: 56–73.
11. Wong ML and Griffiths LG. Immunogenicity in xenogeneic scaffold generation: antigen removal vs. decellularization. *Acta Biomater* 2014; 10: 1806–1816.

12. Wiggenhauser PS, Schantz JT and Rotter N. Cartilage engineering in reconstructive surgery: auricular, nasal and tracheal engineering from a surgical perspective. *Regen Med* 2017; 12: 303–314.
13. Lin H, Yang G, Tan J, et al. Influence of decellularized matrix derived from human mesenchymal stem cells on their proliferation, migration and multi-lineage differentiation potential. *Biomaterials* 2012; 33: 4480–4489.
14. Schantz JT, Hutmacher DW, Lam CX, et al. Repair of calvarial defects with customised tissue-engineered bone grafts II. Evaluation of cellular efficiency and efficacy in vivo. *Tissue Eng* 2003; 9(Suppl. 1): S127–S139.
15. Morrison RJ, Nasser HB, Kashlan KN, et al. Co-culture of adipose-derived stem cells and chondrocytes on three-dimensionally printed bioscaffolds for craniofacial cartilage engineering. *Laryngoscope* 2018; 128: E251–E257.
16. Nyberg E, Rindone A, Dorafshar A, et al. Comparison of 3D-printed poly-ε-caprolactone scaffolds functionalized with tricalcium phosphate, hydroxyapatite, Bio-Oss, or decellularized bone matrix. *Tissue Eng Part A* 2017; 23: 503–514.
17. Kim YS, Majid M, Melchiorri AJ, et al. Applications of decellularized extracellular matrix in bone and cartilage tissue engineering. *Bioeng Transl Med* 2019; 4: 83–95.
18. Kim JY, Ahn G, Kim C, et al. Synergistic effects of beta tri-calcium phosphate and porcine-derived decellularized bone extracellular matrix in 3D-printed polycaprolactone scaffold on bone regeneration. *Macromol Biosci* 2018; 18: e1800025.
19. Mansour A, Mezour MA, Badran Z, et al. Extracellular matrices for bone regeneration: a literature review. *Tissue Eng Part A* 2017; 23: 1436–1451.
20. Nie X and Wang DA. Decellularized orthopaedic tissue-engineered grafts: biomaterial scaffolds synthesised by therapeutic cells. *Biomater Sci* 2018; 6: 2798–2811.
21. Kang H, Peng J, Lu S, et al. In vivo cartilage repair using adipose-derived stem cell-loaded decellularized cartilage ECM scaffolds. *J Tissue Eng Regen Med* 2014; 8: 442–453.
22. Bhumiratana S, Bernhard JC, Alfi DM, et al. Tissue-engineered autologous grafts for facial bone reconstruction. *Sci Transl Med* 2016; 8: 343ra383.
23. Bunnell BA, Flaat M, Gagliardi C, et al. Adipose-derived stem cells: isolation, expansion and differentiation. *Methods* 2008; 45: 115–120.
24. Gilpin A and Yang Y. Decellularization strategies for regenerative medicine: from processing techniques to applications. *Biomed Res Int* 2017; 2017: 9831534.
25. Partington L, Mordan NJ, Mason C, et al. Biochemical changes caused by decellularization may compromise mechanical integrity of tracheal scaffolds. *Acta Biomater* 2013; 9: 5251–5261.
26. Barbosa I, Garcia S, Barbier-Chassefiere V, et al. Improved and simple micro assay for sulfated glycosaminoglycans quantification in biological extracts and its use in skin and muscle tissue studies. *Glycobiology* 2003; 13: 647–653.
27. Choi JS, Kim BS, Kim JD, et al. In vitro cartilage tissue engineering using adipose-derived extracellular matrix scaffolds seeded with adipose-derived stem cells. *Tissue Eng Part A* 2012; 18: 80–92.
28. Rahman S, Griffin M, Naik A, et al. Optimising the decellularization of human elastic cartilage with trypsin for future use in ear reconstruction. *Sci Rep* 2018; 8: 3097.
29. Graham ME, Gratzer PF, Bezuhly M, et al. Development and characterization of decellularized human nasoseptal cartilage matrix for use in tissue engineering. *Laryngoscope* 2016; 126: 2226–2231.
30. Crapo PM, Gilbert TW and Badylak SF. An overview of tissue and whole organ decellularization processes. *Biomaterials* 2011; 32: 3233–3243.
31. Park JS, Chu JS, Tsou AD, et al. The effect of matrix stiffness on the differentiation of mesenchymal stem cells in response to TGF-beta. *Biomaterials* 2011; 32: 3921–3930.
32. Thakkar S, Ghebes CA, Ahmed M, et al. Mesenchymal stromal cell-derived extracellular matrix influences gene expression of chondrocytes. *Biofabrication* 2013; 5: 025003.
33. Zhang Z, Luo X, Xu H, et al. Bone marrow stromal cell-derived extracellular matrix promotes osteogenesis of adipose-derived stem cells. *Cell Biol Int* 2015; 39: 291–299.
34. Gao L, Orth P, Cucchiarini M, et al. Effects of solid acellular type-I/III collagen biomaterials on in vitro and in vivo chondrogenesis of mesenchymal stem cells. *Expert Rev Med Devices* 2017; 14: 717–732.
35. Giuliani N, Lisignoli G, Magnani M, et al. New insights into osteogenic and chondrogenic differentiation of human bone marrow mesenchymal stem cells and their potential clinical applications for bone regeneration in pediatric orthopaedics. *Stem Cells Int* 2013; 2013: 312501.
36. Yamashita A, Nishikawa S and Rancourt DE. Identification of five developmental processes during chondrogenic differentiation of embryonic stem cells. *PLoS One* 2010; 5: e10998.
37. Zhong L, Huang X, Karperien M, et al. The regulatory role of signaling crosstalk in hypertrophy of MSCs and human articular chondrocytes. *Int J Mol Sci* 2015; 16: 19225–19247.
38. Miron RJ and Zhang YF. Osteoinduction: a review of old concepts with new standards. *J Dent Res* 2012; 91: 736–744.
39. Liao HT, Chen JP and Lee MY. Bone tissue engineering with adipose-derived stem cells in bioactive composites of laser-sintered porous polycaprolactone scaffolds and platelet-rich plasma. *Materials (Basel)* 2013; 6: 4911–4929.
40. Brachvogel B, Zaucke F, Dave K, et al. Comparative proteomic analysis of normal and collagen IX null mouse cartilage reveals altered extracellular matrix composition and novel components of the collagen IX interactome. *J Biol Chem* 2013; 288: 13481–13492.